JOURNAL OF GEOPHYSICAL RESEARCH, VOL. 103, NO. C10, PAGES 21,751-21,758, SEPTEMBER 15, 1998

Cyclic loading and creep response of aligned first-year sea ice

D. M. Cole
U.S. Army Cold Regions Research and Engineering Laboratory, Hanover, New Hampshire

R. A. Johnson
College of Letters, Wesleyan University, Middletown, Connecticut

G. D. Durell
U.S. Army Cold Regions Research and Engineering Laboratory, Hanover, New Hampshire

Abstract. Characteristics such as brine and gas porosity and crystallographic features can have a profound impact on the mechanical properties of first-year sea ice. These characteristics vary spatially and temporally, and it is important in the development of constitutive models to address their variability in physically meaningful terms. A program of laboratory experiments on field cores of first-year sea ice has been conducted to aid in the development of such models. A thorough assessment of the bulk physical properties and microstructural characteristics of the ice has been carried out in conjunction with a detailed set of cyclic loading and creep experiments. Methodology was developed to calculate an orientation factor that determines the average shear stress resolved on the basal planes, given the background normal stress. Examination of the constitutive behavior using laboratory cyclic loading and constant load creep experiments revealed that the elastic, anelastic (time-dependent recoverable), and viscous strains varied systematically with the orientation factor. The observations also indicate significant brine porosity effects on the elastic, anelastic, and viscous components of strain. A recently developed constitutive model was expanded to include a frequency- and orientation-dependent viscous straining term, and the model predictions agreed well with the experimental observation.

1. Introduction

This work stems from a joint program of field and laboratory experiments that was conducted under the Office of Naval Research's Sea Ice Mechanics Initiative (SIMI). One component of the SIMI program involved a field investigation of the fracture, creep, creep recovery, and cyclic loading response of aligned first-year sea ice, with emphasis on examining scale effects, developing and verifying constitutive models, and linking laboratory- and field-scale mechanical behavior [*Cole et al.*, 1995]. One aspect of that study focused on examining and modeling the behavior of sea ice under reversed direct-stress and creep loading conditions in the laboratory. To support the constitutive model development and the analysis of in-situ experiments performed in the Alaskan Arctic, field cores were harvested from a test site near Barrow, Alaska, and shipped to the Cold Regions Research and Engineering Laboratory (CRREL) for detailed mechanical properties experiments.

The objective of the experimental work on the field cores was to thoroughly characterize both their physical and mechanical properties and thereby provide the information necessary for the verification of the physically based model. The first-year sea ice examined in the field was highly aligned. To quantify the alignment, a grain-specific fabric analysis was conducted that coupled standard petrographic techniques with a computer-based image analysis. This analysis allowed the calculation of an orientation factor that converts the background normal stress in a particular loading direction to the average shear stress resolved on the basal planes. The mechanical properties of the specimens were determined using zero-mean-stress cyclic loading and creep experiments. The laboratory results showed a good correlation between loading direction relative to the preferred *c* axis direction and the cyclic loading and creep responses, and the orientation factor adequately accounted for the alignment effects on the anelastic and viscous behavior.

Related work on the larger-scale in situ constitutive and fracture experiments and scale effects on fracture appears elsewhere [*Adamson and Dempsey*, 1996; *Dempsey*, 1996; *Mulmule and Dempsey*, 1996; *Adamson et al.*, 1997; *LeClair et al.*, 1997].

2. Background

Arctic sea ice commonly develops a preferred *c* axis direction [*Weeks and Gow*, 1978]. Because of the strong preference for shear deformation and fracture to occur along the basal planes, anisotropy develops in the deformation and fracture of sea ice in proportion to the degree of *c* axis alignment. As a consequence, the quantification of fabric and texture, and the modeling of alignment effects on the mechanical behavior of sea ice have been of interest for some time [*Stander and Michel*, 1989; *Eicken and Lange*, 1991; *Zhan et al.*, 1994; *Cole et al.*, 1996].

C axis alignment effects on the mechanical properties of sea ice have been observed experimentally [*Peyton*, 1966]. Subsequent

Paper number 98JC01265.

efforts [*Borodkin et al.*, 1992; *Richter-Menge*, 1991; *Dempsey*, 1996] have demonstrated that *c* axis alignment produces anisotropy in virtually any measure of mechanical strength and deformation and that the effects can be significant. The compressive strength of first-year sea ice, for example, can vary by a factor of two to three depending on the orientation of the loading axis to the preferred *c* axis direction [*Wang*, 1979; *Richter-Menge*, 1991].

Since interest in sea ice has frequently focused on short-term strength, there have been relatively few creep studies. Although creep has been examined in bending and in uniaxial tension and compression using both in situ field and laboratory specimens of first-year sea ice [*Tabata*, 1958; *Vaudrey*, 1977; *Sinha et al.*, 1992; *Richter-Menge and Cox*, 1995], it is not thoroughly understood. Additionally, since many previous efforts were too extensive for detailed microstructural characterization of individual specimens, there is a paucity of experimental data for verifying physically based constitutive models that incorporate the effects of alignment.

Theoretical analyses of the elastic properties of ice polycrystals have been carried out [*Sinha*, 1989; *Derradji-Aouat et al.*, 1994] that present useful analyses linking the degree of alignment and the pure elastic modulus. It has been demonstrated [*Cole*, 1998] that the polycrystalline moduli calculated by a simple theoretical method [*Sinha*, 1989] agree well with the moduli calculated from ultrasonic velocity measurements of cores of glacier ice when the fabric is known [*Kohnen and Gow*, 1979]. Expressions to account for brine and gas porosity on the elastic modulus of first-year sea ice have been developed and validated [*Cole*, 1996, 1997]. Recent efforts which form the basis of work described here, link detailed microstructural information to the cyclic loading response of first-year sea ice [*Cole and Durell*, 1995a; *Cole et al.*, 1996]. Those results verify that the anelastic relaxation scales with the average shear stress resolved on the basal planes.

3. Experimental Methods

Core specimens of aligned first-year sea ice were harvested in Elson Lagoon, near Barrow, Alaska, at several times during the winter of 1993–1994. The fabric variations with depth in the sheet [*Cole et al.*, 1995] show the development of a strong preferred *c* axis orientation. The cores were transported to the U.S. Army Cold Regions Research and Engineering Laboratory (CRREL) and subjected to a series of creep and cyclic loading experiments [*Cole*, 1993; *Cole and Durell*, 1995a]. Figure 1 shows the orientation of the specimens relative to the preferred *c* axis direction. The cores came from various depths in the ice sheet and represent various stages of refinement in the *c* axis alignment. The specimens as tested were ≈100 mm in diameter, and lengths varied from 250 to 300 mm.

The experimental program called for zero-mean-stress cyclic loading on all specimens, and some were also subjected to monotonic creep and recovery experiments. Cyclic loading frequencies ranged from 10^{-3} to 10 Hz, and peak stress amplitudes ranged from ± 0.1 to ± 0.5 MPa. Typically, three loading cycles of a given frequency and stress level were applied. All specimens were tested at a benchmark temperature of −10°C, and some were subsequently tested at higher temperatures (−7.5, −5, −3°C), but only the −10°C observations are presented and discussed at this time. The creep experiments involved the application of a constant initial stress, generally for a specified period of time, followed by unloading and recovery. Specimens were subjected to compressive and tensile creep stresses of 0.3 MPa in sequence to explore the matter of tension/compression asymmetry. Sets of ±0.2 MPa cycles covering the frequency range noted above were applied before each pair of tension and compression creep loadings and after the final stage. These cyclic loading results provided a means to track the compliance changes resulting from the creep deformation. The applied stresses were kept low in these experiments because of the low tensile strength of the field cores.

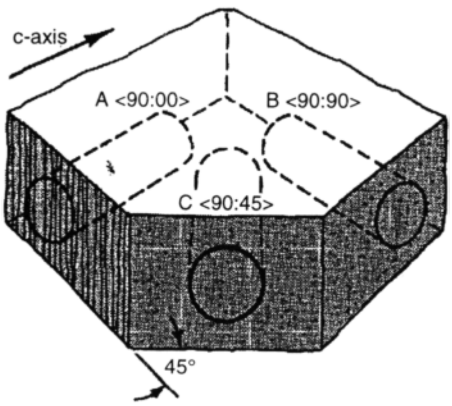

Figure 1. Specimen orientations relative to preferred *c* axis direction. The first letter in the specimen names correspond to Peyton's (1966) designations as shown.

After mechanical testing, appropriately oriented thin sections were obtained and photographed. The constituent grains were numbered on large-format photographs, and the *c* axis orientations were determined with a universal stage. Depending on the grain size of the specimen, from 23 to 50 grains were measured on each thin section. Considering all but one of the specimens, the average area of the grains that were measured amounted to 76 ± 10% of the total area of each thin section. The exception was a fine-grained specimen (4BUB1) for which 49% was measured. The grain numbers and orientations were entered in a computer file that was subsequently read into the analysis program.

Once the orientations for the numbered crystals were obtained, the task was to determine the area of each grain and calculate Schmid factors for the individual grains. The area-weighted average of these factors is the orientation factor Ω required by the model employed in a subsequent section. For a polycrystal of m grains, each with area a_i, total grain area a, with the direction of applied stress making an angle φ_i with the basal plane normal and an angle λ_i with the slip direction, the orientation factor is determined by

$$\Omega = \sum_{i=1}^{m} \frac{a_i}{a} \cos(\lambda_i) \cos(\varphi_i) \tag{1}$$

where

$$a = \sum_{i=1}^{m} a_i \ .$$

The slip direction lies on the basal plane and is assumed to be coplanar with the loading direction and the *c* axis. Random orientation of the grains gives $\Omega = 0.32$. Ω increases to 0.5 for the case of perfectly aligned *c* axes with the axis of loading at 45° to the c axis direction, and decreases to zero for the cases of perfectly aligned ice stressed at 0° or 90° to the *c* axis direction. The procedure next called for digitizing the thin-section photographs and determining the area of the grains of interest using a quantitative image processor (Image Pro Plus). A graphical interface application was developed that invoked functions of the image processor to automatically outline the grains of interest and determine their area as a fraction of the total measured area. Figure 2 shows a typical image after the program has outlined and numbered the grains. The direction of applied stress runs vertically in the figure. The routine requires user input to identify

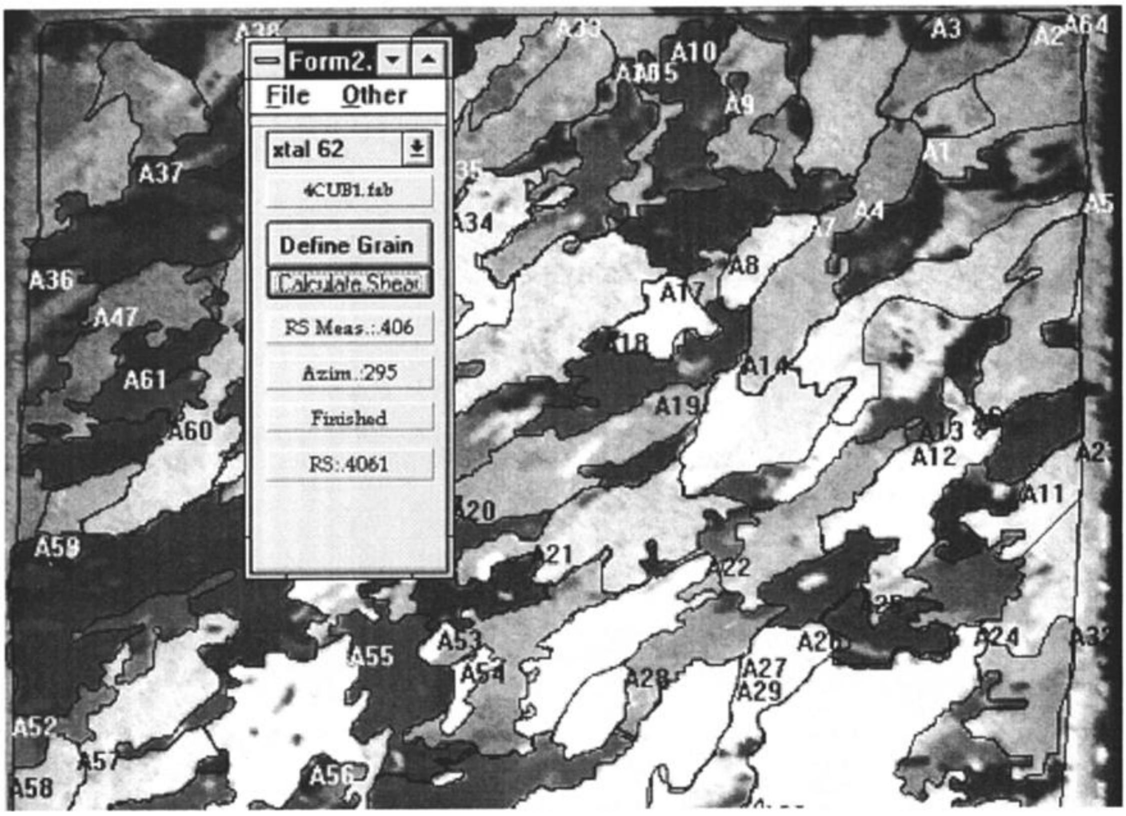

Figure 2. Digitized image of thin section showing numbered grains.

specific grains and occasionally requires user input to establish the location of low-contrast grain boundaries, but otherwise traces them automatically. The program accesses the orientation file mentioned above and calculates area-weighted and unweighted values of Ω.

4. Results

4.1. Orientation Factor

Table 1 gives the results of the orientation factor calculations along with other measurement statistics and specimen properties. Data from Cole et al. [1996] are included for completeness. Figure 3 plots the area-weighted values versus the unweighted values of Ω, along with a line of equality. The area-weighted and unweighted orientation factors agreed to within 10% for 11 of the 16 specimens. However, the area-weighted values were up to 45% higher than the unweighted values in the other specimens. The discrepancies in excess of 10% appeared to be uncorrelated with the depth to the center of the cores or average grain size. The most significant differences occurred in the specimens with <90:45> orientations (see Table 1 notes for explanation of notation). Physical reasoning would indicate that the large discrepancies would occur for specimens having a preponderance of larger grains with a preferred *c* axis direction. This is apparently the case for about one-third of the specimens. However, visual inspection of the thin sections revealed no obvious characteristics common to the specimens exhibiting the large discrepancies.

4.2. Alignment Effects on the Elastic and Anelastic Straining

Figure 4 illustrates typical stress/strain responses of specimens with weighted Ω values of 0.27 and 0.45 for the frequencies indicated. The inelastic straining, as evidenced by the loop widths and areas, increases with Ω. Because the underlying basal slip process is relatively slow, the difference between the two specimens becomes more pronounced as the frequency decreases. The cyclic loading response of the field cores is quantitatively very similar to the behavior observed in laboratory-prepared specimens [*Cole and Durell*, 1995b]. Figure 5 shows the relationship between the effective steady-state modulus and the calculated orientation factors for the applied frequencies.

The moduli are determined from $(\partial\sigma/\partial\varepsilon)_{\sigma=0}$. The values are averages of the moduli calculated for each stress level applied at the indicated frequency for the steady state response (average of the second and subsequent cycles). The curves in this figure are discussed in the section on modeling.

The four data points with the lowest Ω value in Figure 5 are from a laboratory-prepared saline ice specimen (DY1V1, from *Cole and Durell*, 1995b). Since the values of Ω for the field cores did not drop below 0.15, these points are included to help establish the curvature in Figure 5 at lower values of Ω. This specimen is useful because its long axis (and hence the axis of applied stress) runs in the growth direction. Its orientation factor was estimated to be 0.087, assuming a scatter of the *c* axis about the horizontal direction of ±10° (A. Gow, personal communication, 1996).

4.3. Alignment Effects on Viscous Straining

The creep experiments provided information on the effects of alignment on the viscous strain rate and addressed the question of tension/compression asymmetry at small strains. The latter issue was a concern because previous work [*Cole and Durell*, 1995b] noted asymmetry (favoring tensile strain) in the viscous strain accumulated during 10^{-3} Hz loading of laboratory-prepared saline ice. Since

Table 1. Petrographic Analysis Results and Physical Properties of the Test Specimens

Specimen	Number of Measurements	Area Measurement, %	Average Area, mm²	Coefficient of Variation	Orientation Factor Unweighted	Orientation Factor Area Weighted	Salinity, ‰	Porosity, ‰	Density, Mg m⁻³	Depth at Center of Core, m
					*Orientations <90:00>**					
A1MB2†	50	71	167	0.78	0.28	0.27	NA	NA	0.922	0.6
2ALB1†	23	77	120	0.79	0.23	0.20	4.2	29.4	0.912	0.2
4ALB1†	27	77	109	0.66	0.18	0.15	4.0	25.1	0.915	0.2
4AUB1†	38	77	85	NA	0.28	0.28	4.0	20.9	0.919	0.1
A1TB2	35	83	213	0.75	0.27	0.29	3.4	14.5	0.922	0.1
A15B3	47	85	175	0.69	0.24	0.26	3.2	57.6	0.881	0.15
					Orientations <90:90>					
4BLB1†	30	81	111	0.81	0.22	0.20	4.6	40.9	0.903	0.2
4BUB1†	30	49	45	0.68	0.32	0.32	2.9	32.4	0.903	0.1
2BLB1†	30	62	131	0.87	0.26	0.25	4.8	23.8	0.920	0.2
5BLB1†	27	83	103	0.81	0.24	0.23	4.4	53.5	0.890	0.2
5BUB1†	44	74	79	0.66	0.32	0.30	4.8	48.1	0.897	0.1
					Orientations <90:45>					
5CLB1†	27	70	159	0.90	0.31	0.39	3.8	19.8	0.919	0.2
4CUB1†	63	77	121	0.77	0.39	0.41	NA	NA	0.817	0.1
C1BB2†	30	85	276	0.76	0.43	0.43	NA	NA	0.911	1.36
C1MB2	23	92	359	0.75	0.31	0.45	3.4	16.6	0.920	0.74
C133AB3	44	NA	232	0.11	0.34	0 41	2.8	66.1	0.871	1.33
DY1V1‡	NA	NA	NA	NA	0.087§	NA	4.1	49.0	0.893	NA

NA denotes not available.
† Values are from *Cole et al* [1996].
* In this notation, the numbers in brackets indicate the angle, in degrees, between the axis of loading and the growth of the ice and the preferred *c* axis direction, respectively.
‡ Specimen had a vertical orientation [*Cole and Durell*, 1995b].
§ Value is estimated.

there is no generally accepted mechanistic model for the viscous straining of sea ice, the results are presented in a phenomenological context.

The creep experiments generally produced viscous strains between 10^{-4} and 10^{-3} under the –0.3 MPa applied stress and T = –10°C. The viscous strain rate $\dot{\varepsilon}_{visc}$ for each period of loading was determined by dividing the permanent strain, observed after unloading and recovery, by the elapsed time to unloading. Although the viscous strain rate in ice is frequently considered to be constant in the absence of deformational recrystallization, experiments on saline ice (see Figure 6) indicate that $\dot{\varepsilon}_{visc}$ can change noticeably with strain in the early stages of primary creep. Experiments on laboratory-prepared saline ice to be published elsewhere indicate that $\dot{\varepsilon}_{visc}$ may increase or decrease during primary creep depending on stress level and temperature.

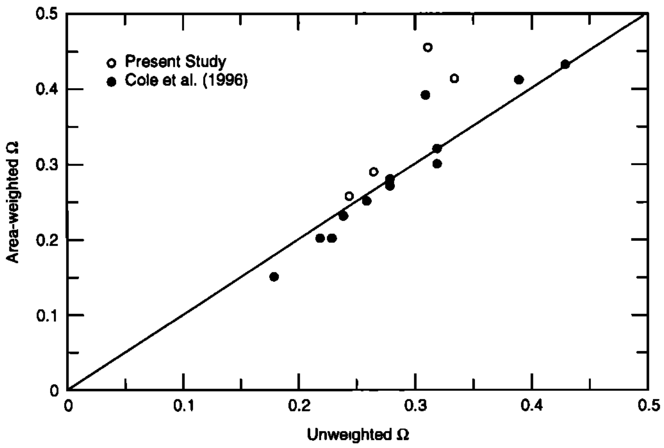

Figure 3. Area-weighted orientation factor versus unweighted factor, with line of equality indicated.

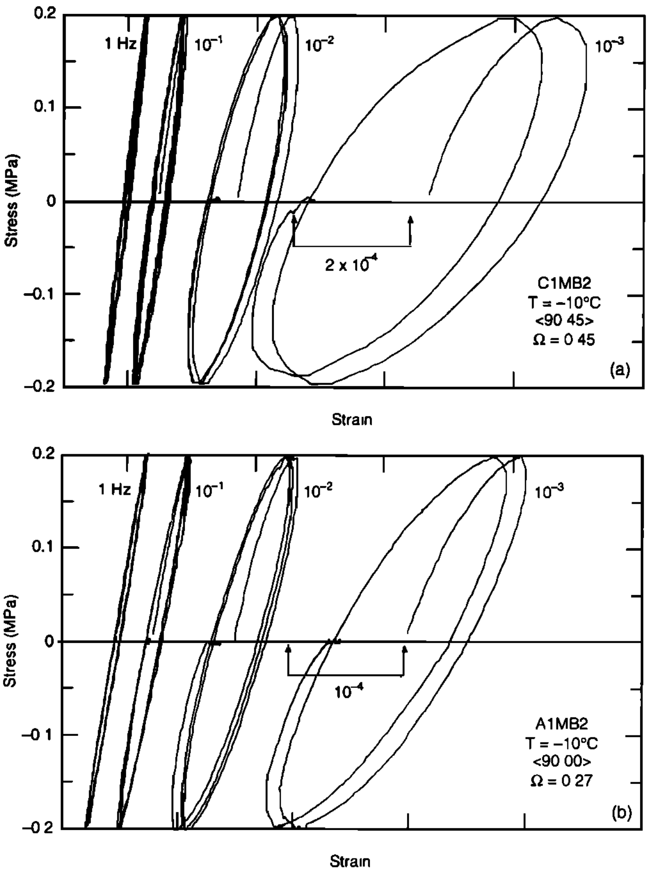

Figure 4. Typical hysteresis loops from field cores with differing orientations to the preferred *c* axis direction. (a) Specimen having a <90:45> orientation and Ω = 0.45. (b) Specimen having a <90:00> orientation and Ω = 0.27.

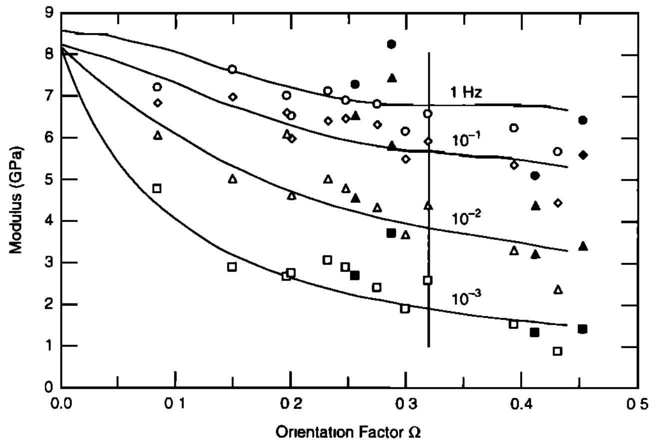

Figure 5. **Modulus versus orientation factor for the test specimens (points), and model predictions as discussed in the text (lines). Cyclic loading frequencies are indicated and the vertical line denotes random orientation. Circles denote 1 Hz, diamonds denote 10^{-1} Hz, triangles denote 10^{-2} Hz, and squares denote 10^{-3} Hz. Open symbols correspond to data from *Cole et al.* [1996].**

Figure 7a shows $\dot{\varepsilon}_{visc}$ as a function of the orientation factor Ω, for the initial creep loading stage applied to eight of the specimens, with the salinities of each specimen indicated. Although somewhat sparse, the data do give an indication of the manner in which the creep rate increases with orientation factor and meltwater salinity. Figure 7b groups three specimens having a salinity of 3.4 ppt but varying orientation factors. Figure 7c shows two specimens, harvested at the same time, having very similar orientation factors but differing salinities. These observations clearly show the tendency for the viscous strain rate to increase with Ω and salinity.

The creep experiments provided no clear indication of tension/compression asymmetry. A strain history effect emerged upon varying the loading sequence (tensile followed by compressive creep loading, and vice versa): the creep rate observed during the second loading was typically higher than during the first loading by approximately 40% regardless of whether the initial loading was tensile or compressive. Specimens subjected to a subsequent set of tensile and compressive creep loadings exhibited a similar trend, but with an increase of approximately 30%. Interestingly, the same specimens exhibited tension/compression asymmetry in the viscous strain when tested under cyclic conditions.

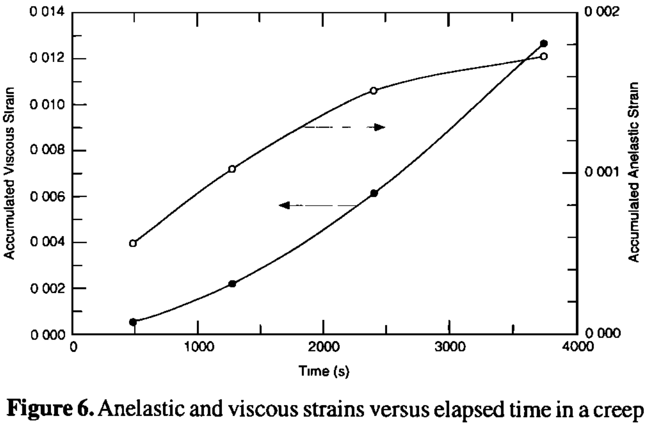

Figure 6. Anelastic and viscous strains versus elapsed time in a creep experiment (σ_{creep} = 0.73 MPa and T = −10°C).

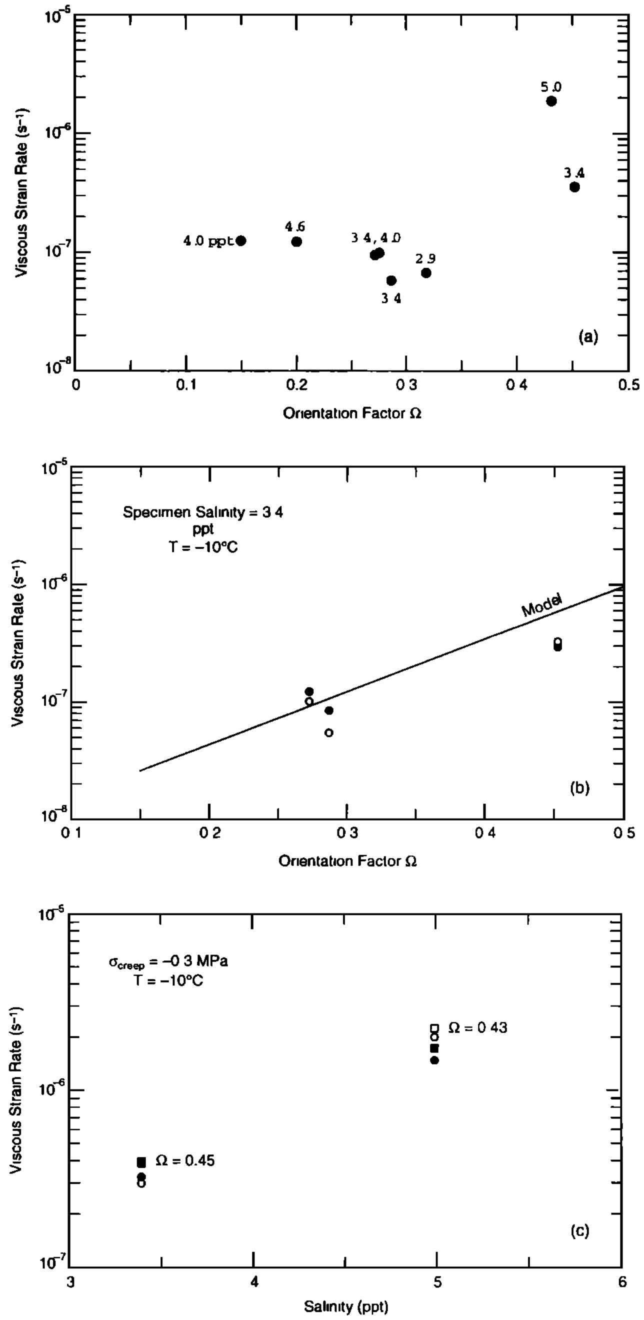

Figure 7. The dependence of viscous strain rate on Ω and salinity for selected specimens. (a) versus Ω with specimen salinities labeled. (b) versus Ω from tests on three specimens having identical salinities (points) and model prediction (line). (c) versus salinity for two specimens with similar Ω values.

5. Modeling

With the inclusion of a viscous straining term, the model of the cyclic loading response of saline ice presented by *Cole* [1995] can be used to quantify the observed orientation effects. The anelastic component of the model incorporates two relaxation processes (basal dislocation glide and grain boundary sliding) to describe the time-dependent recoverable strain of saline ice subjected to cyclic loading. The storage ($D_1[\omega]$) and loss ($D_2[\omega]$) compliances as a function of frequency (ω) are

$$D_1^d(\omega) = D_u^d + \delta D^d \left[1 - \frac{2}{\pi} \tan^{-1} \exp\left(\alpha^d s_i^d\right) \right]$$

$$D_2^d(\omega) = \alpha^d \delta D^d \frac{1}{\exp(\alpha^d s_i^d) + \exp(-\alpha^d s_i^d)}$$

$$D_1^{gb}(\omega) = D_u^{gb} + \delta D^{gb} \left[1 - \frac{2}{\pi} \tan^{-1} \exp(\alpha^{gb} s_i^{gb}) \right] \tag{2}$$

$$D_2^{gb}(\omega) = \alpha^{gb} \delta D^{gb} \frac{1}{\exp(\alpha^{gb} s_i^{gb}) + \exp(-\alpha^{gb} s_i^{gb})}.$$

The superscripts d and gb indicate quantities pertaining to the dislocation and grain boundary relaxations, respectively; $s_i^d = \ln\left(\tau^d \omega\right)$ and $s_i^{gb} = \ln\left(\tau^{gb} \omega\right)$. The dislocation mechanism dominates the anelastic strain in sea ice. Each mechanism has a single activation energy (0.54 and 1.32 eV, for the dislocation and grain boundary relaxations), respectively, and a distribution in relaxation time. The temperature dependence enters through the central relaxation times τ^i for each mechanism.

The anelastic strain component of the model is linear and accounts for orientation effects under uniaxial loading with the orientation factor Ω that enters the model through the quantity δD^d given by

$$\delta D^d = \frac{\rho \, \Omega b^2}{K} \tag{3}$$

where ρ is the mobile dislocation density on the basal planes, b is the Burgers vector and K is an experimentally determined restoring stress constant. The model predictions shown here use the relaxation parameters reported in *Cole* [1995]. The calculations ignore potential anisotropy in the grain boundary sliding since the overall contribution of that mechanism is small.

The purely elastic modulus E of the inclusion-free ice is calculated from the temperature-dependent single crystal compliances, an expression that yields the single crystal modulus for an arbitrary loading direction [*Stephens*, 1958], and an expression presented by Sinha [1989] to calculate the unrelaxed modulus of aligned ice. This calculation yields a temperature- and fabric-dependent modulus of the inclusion-free material, $E(T,\angle)$. *Cole* [1996] demonstrated that gas porosity v_a effects on the modulus can be expressed with a factor of $(1-3v_a)$. The brine porosity v_b effects on the elastic behavior were addressed with an empirical factor $f(v_b)$ which is based on the experimental data of *Slesarenko and Frolov* [1974]. The pure elastic compliance used in the model calculations is the inverse of the elastic modulus given by

$$E = E(T,\angle) \times (1-3v_a) \times f(v_b). \tag{4}$$

The curves in Figure 5 are the model predictions obtained using the average physical properties of the specimens. To simplify Figure 5, the model predictions for $\Omega < 0.32$ were calculated for the <90:00> orientation only. Since there is a slight elastic anisotropy between the <90:00> and <90:90> orientations, the moduli for the latter orientation, if plotted, would fall increasingly lower than the plotted curve as Ω approaches zero. The strains for $\Omega > 0.32$ were calculated for the <90:45> orientation. The predictions based on either orientation agree for $\Omega = 0.32$, as they should, because that value corresponds to the isotropic case. Since the cyclic loading response is governed primarily by the elastic and anelastic response for the prevailing conditions, the results indicate that the model predictions for these components of strain are in good agreement with the experimental observations at the frequencies examined.

Figure 8a compares the strain-time response from one of the field specimens with the model predictions for the loading conditions indicated and Figure 8b decomposes the predicted cyclic loading response into its elastic, anelastic, and viscous components. The elastic strain is in-phase with the applied stress, the anelastic strain lags by an amount determined by the internal friction, and the viscous strain is 90° out of phase with the applied stress. The initial transient in the viscous strain is tentatively handled using the method employed by *Cole* [1995] to calculate the transient behavior of the anelastic strain.

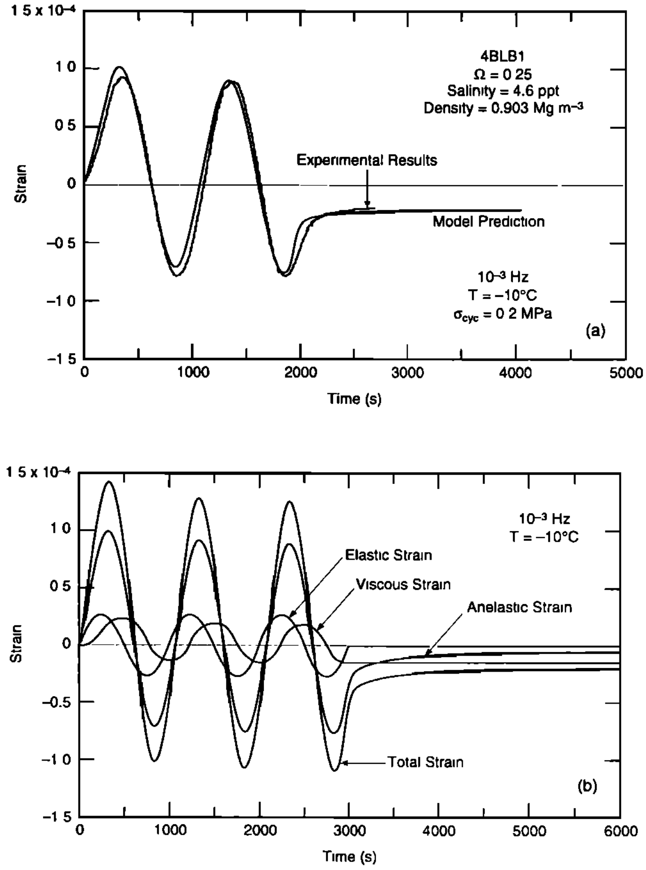

Figure 8. Example model predications of the cyclic loading response of aligned first-year sea ice. (a) Comparison of total strain versus time for specimen 4BLB1 and the test conditions indicated. (b) Decomposition of the model predictions into its elastic, anelastic and viscous components.

The creep data were analyzed with a power law [*Glen*, 1958] formulation:

$$\frac{\dot{\varepsilon}_{\text{visc}}}{\dot{\varepsilon}_0} = A(\Omega \frac{\sigma}{\sigma_0})^n \exp\left(-\frac{Q_{\text{creep}}}{kT}\right) \tag{5}$$

where n = 3, σ is the background normal stress in megapascals, Q_{creep} = 0.7 eV, k is Boltzmann's constant, and T is the temperature in kelvins. The constants $\dot{\varepsilon}_0 = 1\,\text{s}^{-1}$ and σ_0 = 1 MPa are introduced to produce a dimensionless creep parameter A.

Calculations of the parameter A for the creep experiments (Figure 9) showed it to increase markedly with brine porosity. The calculations for Figure 8b employed a value of $A = 5 \times 10^{10}$, which was determined from a creep experiment performed on the specimen subsequent to the cyclic loading experiment. Under steady-state sinusoidal loading at a frequency ω and a peak axial stress of σ, the viscous strain component is given by

$$\varepsilon_{\text{visc}}(t) = \omega^{-1} \left(\Omega \frac{\sigma}{\sigma_0} \right)^n A \exp\left(-\frac{Q_{\text{creep}}}{kT} \right) \left\{ -\frac{1}{3} \cos(\omega t) \left[\sin^2(\omega t) + 2 \right] \right\} \tag{6}$$

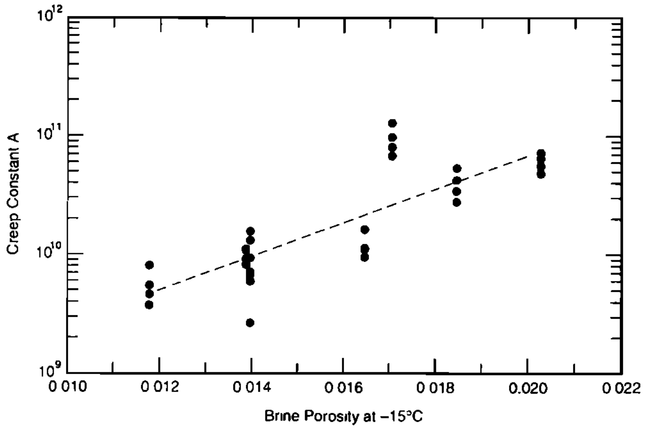

Figure 9. Creep constant A versus brine porosity (at −15°C). Each group of points reflects the range in A found for a specimen subjected to the sequence of tensile and compressive creep loadings described in the text.

The model calculations used $\Omega = 0.25$, as determined from the orientation analysis, and an elastic modulus of 7.9 GPa as determined from (3). The anelastic compliance of 5.45×10^{-10} Pa^{-1} was determined from the relationship presented by Cole [1998]. Figure 7b indicates that the limited observations are in reasonable agreement with the predicted Ω^3 dependency.

The relationship between the specimen's physical properties (salinity and density) and the anelastic compliance, which is based on the results of laboratory-prepared specimens, adequately predicts the anelastic strain observed in the typical field core specimen shown in Figure 8. The total predicted strain is slightly higher than the observed strain during the first quarter cycle and at the start of the recovery period (see Figure 8a) but is otherwise in good agreement. This indicates that the core specimen is exhibiting a relaxation time distribution that is shifted to slightly longer times than found for the laboratory-prepared specimens upon which the model is based.

6. Discussion

The foregoing observations verify that the anelastic and viscous straining of aligned sea ice specimens are well correlated with an orientation factor that reflects the shear stress resolved on the basal planes. In comparing the response of the specimens with the highest and lowest alignment factors, typical alignment effects account for reductions in modulus observed under cyclic loading of 26% at 1 Hz and 70% at 10^{-3} Hz. The smaller effect at 1 Hz results from the reduced contribution of the dislocation relaxation process. The effects of elastic anisotropy on the modulus are relatively small and virtually disappear at lower frequencies when the dislocation contribution becomes large.

Beyond the time needed for standard fabric work, an additional 1 to 2 hours per specimen are required to calculate the area-weighted value of Ω. It is therefore of practical interest to consider when area-weighted values are necessary. Area weighting is clearly unimportant for material with uniform grain size. However, the area-weighting method would prove useful in the analysis of specimens that contain an insufficient number of grains to produce polycrystalline behavior. For cases not requiring an area-weighted orientation factor, the model can calculate the appropriate value of Ω based simply on the half-cone angle (half of the included angle of points on a pole plot) and the angle between the preferred c axis direction and the direction of applied stress. It is especially important to accurately determine Ω for the viscous strain calculation because of the third-power dependence (equation (5)) on this quantity.

The ability of the model to predict the cyclic loading response of the field cores, as well as in situ behavior, is still under investigation. However, thus far, the predictions of the model, which is based on the mechanical behavior of laboratory-prepared saline ice, show an encouraging agreement with the experimental observations on the field cores. It is noteworthy that the model produces reasonable predictions of the elastic and anelastic response of the core specimens based only on their physical properties. There are no free-floating parameters in the model, and no adjustments of other quantities were made for the calculations.

The differences in the anelastic relaxation time distributions of the model and experimental data are a point of interest. The relaxation time distribution, which controls the width of the anelastic relaxation peak, is influenced by microstructural characteristics and thus might be expected to exhibit some variability. To account for the peak-broadening effect of the relaxation time distribution, the model employs the peak width parameter $\alpha^d = 0.54$ for the dislocation relaxation process. The value of α^d was determined from a statistical analysis of data from laboratory-prepared specimens [*Cole*, 1995]. Similar analyses of the cyclic loading response of both the field cores and the in situ specimens [*Adamson and Dempsey*, 1996] are being conducted to determine whether the laboratory-based value of α^d accurately predicts larger-scale behavior.

Values of the viscous straining parameter A obtained from the creep experiments on the field cores are comparable to values obtained by the authors for laboratory specimens with similar salinities and densities. The model accurately predicts the viscous strain during cyclic loading using a value of the parameter A determined from a subsequent creep experiment on the same specimen. This not unexpected result serves as a check on the internal consistency of the model, but obviously lacks generality. A short-term goal of the work in this regard is to develop a simple empirical relationship between the creep constant A and the brine porosity v_b. The long-term intent is to develop a physical understanding of this relationship.

An important peripheral issue is the observation that the viscous strain rate increased during primary creep, following a similar trend in the level of anelastic straining. Previous work on laboratory-prepared specimens [*Cole*, 1993] indicated that creep deformation can significantly increase the dislocation population as indicated by the anelastic compliance. It is important to note that this effect occurs in the absence of a significant degree of microcracking. Since both the anelastic compliance and the viscous strain rate were apparently reaching a plateau value during primary creep in the experiment noted above, there is some indication that basal dislocation density plays a role in both straining processes. The tensile and compressive creep experiments on the field cores showed essentially the same behavior: the anelastic compliance and the viscous strain rate both increased with prior straining. If further observations bear this out, it will be necessary to reexamine the assumption that the viscous strain rate, and thus the value of A, remains constant during the early stages of primary creep in sea ice.

7. Conclusions

For the case of field cores of aligned first-year sea ice examined at −10°C, the experimental work and analysis presented herein lead to the following conclusions:

1. The method presented to calculate an area-averaged orientation factor adequately characterized the effects of c axis alignment on the cyclic loading response.

2. A simple mean orientation factor agrees with the area-weighted orientation factor to within 10% for the majority (approximately two thirds) of cases examined, but differences between the two can reach 45%.

3. A limited number of observations indicated that the orientation factor discussed in the text properly scales the power law expression for the viscous straining.

4. For the range of physical properties examined, the viscous strain rate increased markedly with brine volume in experiments with $\sigma_{creep} = \pm 0.3$ MPa.

5. There was no consistent evidence of tension/compression asymmetry in the uniaxial creep behavior of the core specimens.

6. There was evidence of a strain history effect on the viscous creep rate, with the implication that the viscous creep rate may not be constant in the early stages of deformation.

7. An anelastic straining model based on laboratory-prepared saline ice specimens adequately predicted the frequency and fabric dependence of the cyclic loading response of field cores of aligned, first-year sea ice.

In closing, it is noted that the viscous strain rate/brine porosity relationship, strain history effects on both the anelastic and viscous straining, and the characteristics of the relaxation time distribution for the field cores are subjects of ongoing analyses. As of this writing, the verification of the model with larger-scale, in situ cyclic and creep loading experiments is in progress.

Acknowledgments. This work was conducted under the Office of Naval Research, Sea Ice Mechanics Initiative, grants N0001495MP30001 and N0001496MP30021. The authors express their appreciation to Thomas Swean, Thomas Curtin and Yapa Rajapakse of ONR for their support. We also gratefully acknowledge Nancy Perron for her help in specimen preparation, petrography, and physical properties determinations.

References

Adamson, R.M. and J.P. Dempsey, Large-scale in-situ Arctic cyclic, creep recovery and fracture experiments, paper presented 13th International Symposium on Ice, Beijing, Int. Assoc. for Hydraulic Res., 1996.

Adamson, R.L., L.H. Shapiro, and J.P. Dempsey, Core-based SCB fracture of aligned first-year sea ice (Phases III & IV), *J. of Cold Reg. Eng., 11,* 30–44, 1997.

Borodkin, V.A., V.P. Gavrilo, S.M. Kovalev and G.A. Lebedev, Influence of structural anisotropy of sea ice on its mechanical and electrical properties paper presented at Second International Offshore and Polar Engineering Conference, San Francisco, 1992.

Cole, D.M., The effect of creep on the constitutive behavior of saline ice at low strains, In *Ice Mechanics 1993,* vol. 163, pp. 261–272, Appl. Mech. Div., Am. Soc. Mech. Eng., New York, 1993.

Cole, D.M., A model for the cyclic loading of saline ice subjected to cyclic loading. *Philos. Mag. A, 72,* 231–248, 1995.

Cole, D M., On the relationship between the physical and mechanical properties of sea ice, paper presented 13th International Symposium on Ice, Beijing, Int. Assoc. for Hydraulic Res., 1996.

Cole, D.M., Modeling the cyclic loading response of first-year sea ice, *Int. J. Solids Struct., 35,* 4067–4075, 1998.

Cole, D.M. and G.D. Durell, The effect of c axis alignment on the constitutive behavior of sea ice at low strains, in *Ice Mechanics-1995, AMD,* vol. 207, 189–199, Appl. Mech. Div., Am. Soc. Mech. Eng., New York, 1995a.

Cole, D.M. and G.D. Durell, The cyclic loading of saline ice, *Philos. Mag. A, 72,* 209–230, 1995b.

Cole, D.M., L.H. Shapiro, W.F. Weeks, J.P. Dempsey, R.M. Adamson, V.F. Petrenko, and O.V. Gluschenkov, Overview of a recent program on sea ice mechanics, *J. Cold Regions Eng., 9,* 219–234, 1995.

Cole, D.M., R.A. Johnson and G.D. Durell, The cyclic loading response of aligned first-year sea ice, paper presented 13th International Symposium on Ice, Beijing, Int. Assoc. for Hydraulic Res., 1996.

Dempsey, J.P., Scale effects on the fracture of ice, in *The Johannes Weertman Symposium,* edited by R.J. Arsenault, et al., pp. 351–361, Miner., Metals and Mater. Soc., Warrendale, Pa, 1996.

Derradji-Aouat, A., N.K. Sinha and E. Evgin, Practical elastic moduli for polycrystalline ice, paper presented at 13th Intl. Conf. Offshore Mech. and Arctic Engineering, Houston, Am. Soc. Mech. Eng., 1994.

Eicken, H., and M.A. Lange, Image analysis of sea-ice thin sections: A step towards automated texture classification, *Ann. Glaciol., 15,* 204–209, 1991.

Glen, J.W., The flow law of ice: A discussion of the assumptions made in glacier theory, their experimental foundations and consequences, paper presented at Symposium of Chamonix on the Physics of the Movement of Ice, Intl. Assoc. Hydrol. Sci., 171–183, 1958.

Kohnen, H. and A.J. Gow, Ultrasonic velocity investigations of crystal anisotropy in deep ice cores from Antarctica, *J. Geophys. Res., 84,* 4865–4874, 1979.

LeClair, E.S., R.M. Adamson and J.P. Dempsey, Core-based SCB fracture of aligned first-year sea ice (Phase VI), *J.Cold Reg. Eng., 11,* 45–58, 1997.

Mulmule, S.V., and J.P. Dempsey, Nonlinear fracture theories for freshwater and sea ice, paper presented 13th International Symposium on Ice, Beijing, Int. Assoc. for Hydraulic Res., 1996.

Peyton, H.R., Sea ice strength, Report UAG-182, 187 pp., Geophys. Inst., Univ. of Alaska, Fairbanks, 1966.

Richter-Menge, J.A., Confined compressive strength of horizontal first-year sea ice samples, *J. Offshore Mech. Arct. Eng., 113,* 344–351, 1991.

Richter-Menge, J.A. and G.F.N. Cox, The creep of saline ice at low stresses and high temperatures, paper presented at 5th Intl. Conf. on Port and Ocean Engineering Under Arctic Conditions, The Hague, Netherlands, June 11–16, 1995.

Sinha, N.K., Elasticity of natural types of polycrystalline ice, *Cold Reg. Sci. Technol., 17,* 127–135, 1989.

Sinha, N.K., C. Zhan, and E. Evgin, Creep of sea ice. Paper presented at 11th Intl. Conf. on Offshore Mechanics and Arctic Engineering, Calgary, Am. Soc. Mech. Eng., 1992.

Slesarenko, Y.E., and Frolov, A.D., Comparison of elasticity and strength characteristics of salt-water ice, Proc. Paper presented at Symposium on Ice and Its Action on Hydraulic Structures, Int. Assoc. for Hydraulic Res., 1974.

Stander, E., and B. Michel, The effect of fluid flow on the development of preferred orientations in sea ice: Laboratory experiments, *Cold Reg. Sci. Technol., 17,* 153–161, 1989.

Stephens, R.W.B., The mechanical properties of ice, II, The elastic constants and mechanical relaxation of single crystal ice, *Adv. Physics, 7,* 266–275, 1958.

Tabata, T., Studies on visco-elastic properties of sea ice, Arctic sea ice, Pub. 598, pp. 139–147. Nat. Acad. of Sci. Nat. Res., Washington, D.C., 1958.

Vaudrey, K.D., Ice-engineering—Study of related properties of floating sea-ice sheets and summary of elastic and viscoelastic analyses, Tech. Rep. R860, 81 pp., Nav. Civ. Eng. Lab Port Hueneme, Calif, 1977.

Wang, Y.S., Crystallographic studies and strength tests of field ice in the Alaskan Beaufort Sea, paper presented 5th Intl. Conf. on Port and Ocean Engineering Under Arctic Conditions, The Hague, Netherlands, June 11–16, 1979.

Weeks, W.F. and A.J. Gow, Preferred crystal orientations in the fast ice along the margins of the Arctic Ocean, *J. Geophys. Res., 83,* 5105–5121, 1978.

Zhan, C., N.K. Sinha, and E. Evgin, Effect of crystal orientation on behavior of columnar-grained sea ice, paper presented at 13th Intl. Conf Offshore Mech. and Arctic Engineering, Houston, Am. Soc. Mech. Eng., 1994.

D. M. Cole, Applied Research Division, U.S. Army Cold Regions Research and Engineering Laboratory, 72 Lyme Road, Hanover, NH 03755-1290. (email:dmcole@crrel.usace.army.mil)

G. D. Durell, Engineering Resources Branch, U.S. Army Cold Regions Research and Engineering Laboratory, 72 Lyme Road, Hanover, NH 03755-1290. (email:gdurell@crrel.usace.army.mil)

R. A. Johnson, Wesleyan University, Wesleyan Station Box 4540, 22 Church St., Middletown, CT 06459-4540. (email: rjohnson@mail.wesleyan.edu

(Received May 12, 1997; revised January 22, 1998; accepted January 28, 1998.)